Absence of a guiding effect and charge transfer in the interaction of keV-energy negative ions with Al_2O_3 nanocapillaries

Lin Chen, Yanling Guo, Juanjuan Jia, Hongqiang Zhang, Ying Cui, Jianxiong Shao, Yongzhi Yin, Xiyu Qiu, Xueyang Lv, Guangzhi Sun, Jun Wang, Yifeng Chen, Fayuan Xi, and Ximeng Chen*

School of Nuclear Science and Technology, Lanzhou University, 730000 China

(Received 13 June 2011; published 22 September 2011)

In this work, the efficient electron loss process was observed for the transmission of 10- to 18-keV Cu^- and Cl^- ions through Al_2O_3 nanocapillaries. The fractions of the scattered particles were simultaneously measured using a position-sensitive microchannel plate detector. The neutrals were guided through the capillary via multiple grazing scattering. In particular, the scattered Cl^- ions were observed in the transmission, whereas no Cu^- ion was formed. In contrast to highly charged ions, these results support strongly the fact that the scattering events dominate the transport of negative ions through the nanocapillaries and that there is no direct evidence for the formation of *negative* charge patches inside the capillaries which are able to repulse and guide negative ions efficiently.

DOI: 10.1103/PhysRevA.84.032901 PACS number(s): 79.20.Rf, 34.50.Fa, 68.49.Sf

I. INTRODUCTION

Recently, interactions between charged ions and insulator surfaces have attracted considerable attention, in particular, increasing interest in the growing field of insulating nanocapillary transmission. Stolterfoht *et al.* first reported the guiding effect in slow highly charged ions (HCIs) of 3 keV Ne^{7+} through insulating nanocapillary foils of polyethylene terephthalate (PET) [1]. The so-called guiding effect is defined as that HCIs preserving their incident charge state and kinetic energy can be transmitted through the insulating nanocapillary foil without suffering close collisions with the capillary walls, even when they are tilted to an angle significantly larger than the geometric angle given by the capillary aspect ratio. Due to a series of recent works [2–6] (and references therein) on time or deposited-charge evolution of the angular distribution of the guided ions, this guiding phenomenon has been ascribed to the self-organizing process of charge patches being formed on the inner wall of the capillary. During the pre-equilibrium period the guided ions are affected by sequentially formed charge patches [4,6], whereas the ions are guided through the capillary axis predominantly by the first charge patch formed at the entrance region of the capillaries under the equilibrium condition, and sequential charge patches may remain within the inner walls. The resulting oscillation structures have been studied in detail for the transmitted angular distribution. Very recently, the extended work on the formation of neutrals in 3 keV Ar^{7+} transmitted through PET nanocapillaries has been reported [6], where the emission of neutrals always occurs before the appearance of the guided ions and then coexists with them. This work demonstrates that the charge exchange process indeed takes place and maintains the continuous charge deposition in the capillary.

Previously, we reported the experimental results for multiply charged ions transmitted through insulating Al_2O_3 nanocapillaries [7,8], where the similar guiding phenomenon was observed. On the other hand, the negative ion transmission has not been the subject of similar attention as compared to the large amount of research for slow HCIs. Very recently, we reported the transmission of 18 keV O^- ions through insulating Al_2O_3 nanocapillaries [9], which was devoted to studying the similar characteristic of the guiding effect as expected, since it is well known that both negative and positive ion beams can make the insulating surface charged. So far, very little effort has been devoted to the dynamics of the negative ion transmission [9], for which many questions remain unanswered. One of the motivations of the present study is to further examine one of these questions, namely the charging-up phenomenon, by using different types of negative ions with low ion dose rates.

In the metallic surface case, negative-ion formation involves a transition of an electron from occupied levels of the valence band to the anion level of the projectile. The latter one is downward shifted due to image potential effects [10]. Departing from the surface, the negative ion quickly decays via resonant ionization and becomes an atom. As opposed to metallic surfaces, the surprising high survival of negative ions has been observed in the case of insulator surfaces, where negative-ion formation is favored by the Madelung potential [11] and the subsequent electron loss is suppressed by the wide band gap of the insulator [12]. However, for H, O, and F atoms and anions scattered from an MgO (100) surface in grazing incidence, Ustaze *et al.* [13] reported the observation of the existence of an efficient electron loss channel, in which electron loss due to the transfer of electrons to the cation Mg site was proposed. On the theoretical side, the binary encounter model developed by Deutscher *et al.* [14] gave a good description of the negative-ion production at lower velocities [13] but failed at larger velocities where the efficient electron loss channel exists. The study of the negative ions transmitted through insulating nanocapillaries may provide a means to probe the electronic properties of the nanocapillaries, i.e., the charge-transfer properties. Thus, in the 10- to 18-keV energy range studied, the present study is of interest and likely to provide a new insight into understanding the electron loss process for negative ions through insulating nanocapillaries.

In this work, we report the negative and positive ion formation during transmission of 10- to 18-keV Cu^- and Cl^- ions through Al_2O_3 nanocapillaries in comparison with

*Corresponding author: chenxm@lzu.edu.cn

previous O^- results. Similarly, as for O^-, with the increase of the tilt angle, grazing scattering on inner walls of the capillary plays the main role, meanwhile, the directly transmitted beam dramatically reduces and finally disappears at large tilt angles. As a result, the scattered neutrals are guided through the capillaries via multiple grazing scattering. On the other hand, the significant difference is observed in the charge exchange process. For Cu^- and Cl^- projectiles, the fraction of scattered neutrals increases with increasing the tilt angle and is as high as 80% when the tilt angle is larger than 2.5°. The positive ion fraction was found to be up to 40% for Cu^-, as well as 10% for Cl^- projectiles. In particular, we did not observe the formation of negative Cu^- ions, which differs from the cases of O^- and Cl^- ions.

II. EXPERIMENTS

The experiment was carried out in the Institute of Nuclear Physics at Lanzhou University. The experimental apparatus used for the present measurements can be found elsewhere [9]. Briefly, Cu^- (Cl^-) ions were produced in the cesium sputter ion source and collimated to a diameter of 3 mm by two sets of 1.5×1.5 mm^2 collimators 75 cm apart before entering a high vacuum chamber. The pressure was kept below 2.5×10^{-5} Pa both in the beam line and in the chamber. The angular divergence of the primary beam was about 0.23° (full width at half maximum, FWHM) for all measurements. The charge states of transmitted ions were analyzed by a parallel-plate electrostatic analyzer and then recorded using a one-dimensional position sensitive microchannel plate detector (1D PSMCP). Typically, ion currents as low as a few tens of picoamps were used, since at higher currents the MCP detector system saturates. It, therefore, always takes several thousand seconds to accumulate the count when the target is tilted to large angles. Furthermore, the experimental data were reproduced via a series of measurements.

The Al_2O_3 nanocapillary foil used in our measurements was located at the center of the chamber, which contained a dense distribution of capillary arrays with a diameter of 50 nm and length of 10 μm (corresponding to an aspect angle of ~0.29°). Both front and back surfaces were coated with gold to avoid macroscopic charging-up of the surfaces during ion beam exposure. The sample can be rotated around one vertical axis by the horizontal tilt angle ψ which is referred as an angle between the capillary axes and the incident beam. The deflection angle θ is related to the angular distribution of transmitted particles on the detector with respect to the incident beam direction, and θ is in the same plane as the tilt angle.

It should be noted that the capillary nonparallelism does indeed exist in the present measurements. In the earlier work [9], the directly transmitted beam has been clearly observed even at a tilt angle of about 2°, where it was ascribed to a practical problem of the target preparation. We aligned the capillary to the incident beam by adjusting the tilt angle in steps of 0.2°. The position where the highest count rate of transmitted particles was reached was chosen as the zero position ($\psi = 0°$). Throughout this procedure, the ion beam current was kept very low to avoid any obvious charging up of the capillaries.

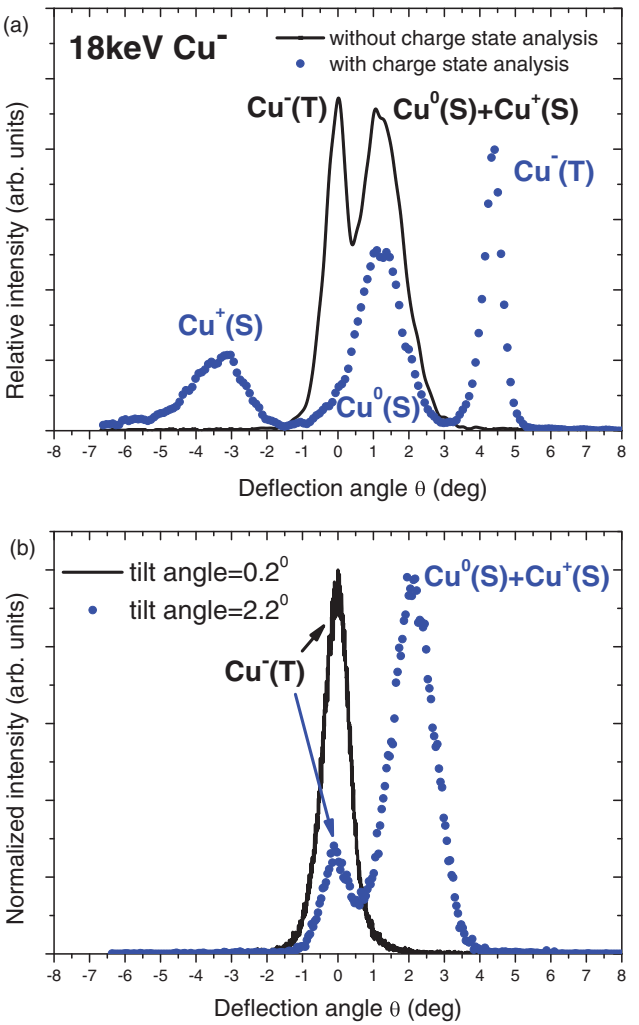

FIG. 1. (Color online) (a) Angular distribution of 18 keV Cu^- ions transmitted through Al_2O_3 nano-capillaries at a tilt angle of 1.6° with (without) charge state analysis; (b) Normalized transmitted intensities of 18 keV Cu^- ions as a function of the deflection angle without charge state analysis: tilt angle $\psi = 0.2°$ (black line) and 2.2° (solid circles). The intensity of the *S* peak for $\psi = 2.2°$ is normalized to that of the *T* peak for $\psi = 0.2°$.

III. RESULTS

In Fig. 1(a), the angular distribution of 18-keV Cu^- ions is presented for Al_2O_3 nanocapillaries at a tilt angle of 1.6°. Two peaks are observed in the angular distribution spectrum without charge state analysis. The similar double-peak structure has been observed in the earlier study [9] and the same definitions have also been adopted here. The sharper peak near 0° is defined as the "*T*" peak, and the other one at about 1.6° is the "*S*" peak. With charge-state analysis by use of electrostatic parallel plates, it is found that the *T* peak consists of Cu^- ions resulting from direct transmission without any collisions with inner walls and that the *S* peak consists of scattered Cu^0 and a smaller amount of Cu^+ ions, both of which are scattered from the inner walls. The angular width, the FWHM, is about 0.6° for the *T* peak and is significantly broader for the *S* peak. In Fig. 1(b), as the tilt angle decreases to zero, the deflection angle position of the *T* peak does not change,

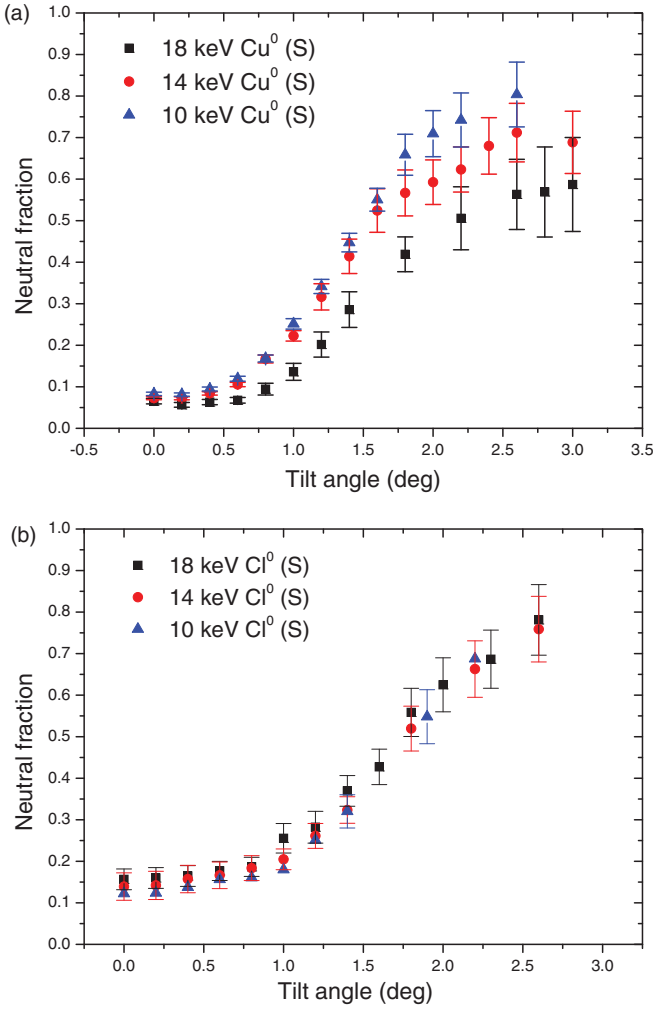

FIG. 2. (Color online) Neutral fraction of scattered Cu^0 (a) and Cl^0 (b) from the *S* peak as a function of the tilt angle for different incident energies.

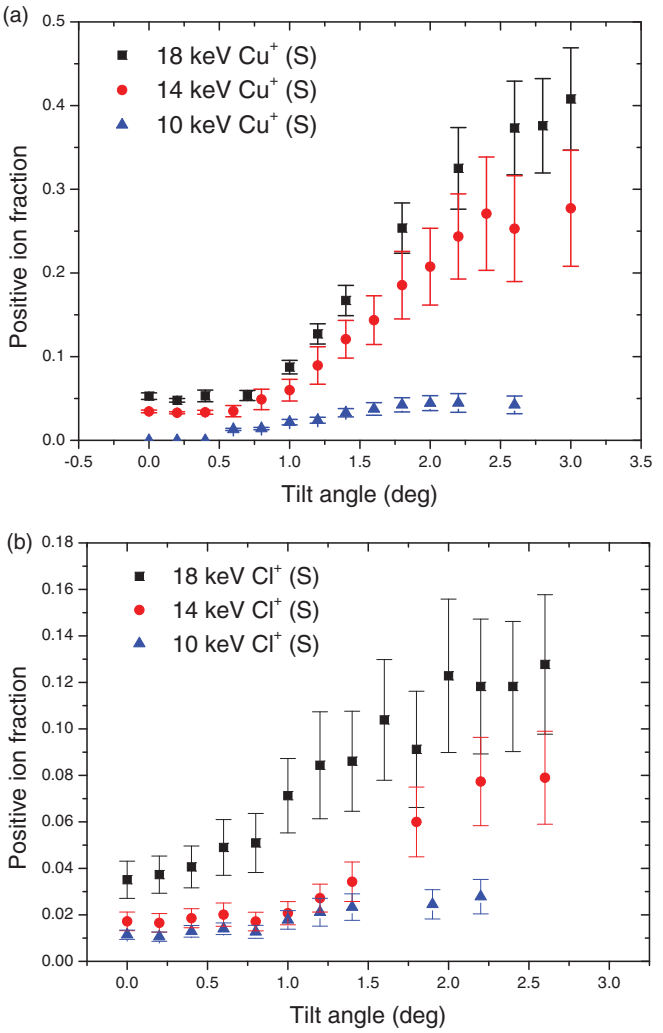

FIG. 3. (Color online) Positive ion fraction of scattered Cu^+ (a) and Cl^+ (b) from the *S* peak as a function of the tilt angle for different incident energies.

while *S* is seen to shift to smaller angles. Meanwhile, the intensity of *T* grows while *S* decreases, and almost disappears, at a tilt angle of 0°. In contrast, for the tilt angle above 2.4°, the *T* peak almost disappears and the transmitted particles almost come from the *S* peak.

The interesting feature of our work is related to charge exchange processes in the negative-ion transmission. The fraction of scattered particles is defined by the ratio of the *S* peak component to the total transmitted particles (i.e., $T + S$). In Fig. 2, the fraction of scattered neutrals remains constant below 0.5° and then increases rapidly, after which it seems to tend to saturation as the tilt angle becomes larger than 2.5°. The neutral fractions for Cu are almost the same for different incident energies at smaller tilt and are obviously dependent on incident energy at larger tilt angles, where the larger the incident energy the smaller the fraction. In contrast, in the case of Cl, the fraction may be independent of the incident energy.

The positive ion fraction is shown Fig. 3 as a function of the tilt angle. In general, the fraction increases with the increase of both the tilt angle and the incident energy. The charge fraction plateaus are observed for both the Cu and Cl projectiles at the lowest tilt angles. A threshold for the tilt angle is observed for 10-keV Cu^- incidence, similarly to the oxygen case [9]. The onset of the rise of the fraction appears at about 0.5°. In addition, the fraction of Cu is generally larger than Cl and O over the whole tilt angle range studied.

In Fig. 4, the negative-ion fraction of scattered Cl^- ions (from the *S* peak) is as high as 10%, comparable to the positive ion fraction. It increases with increasing the tilt angle. On the contrary, for Cu^- ion incidence, we have not observed the scattered Cu^- ions, as shown in Fig. 1.

IV. DISCUSSION

A. Neutralization of negative ions

In our experiments, the intensity of the *T* peak is still observed at around zero deflection angle and appears immediately without time delay after the beam is turned on. The equilibrium time is so short that no change during the pre-equilibrium period can be observed in the measurements.

The direct transmission of negative ions is probably more related to geometric conditions. It is the consequence of the

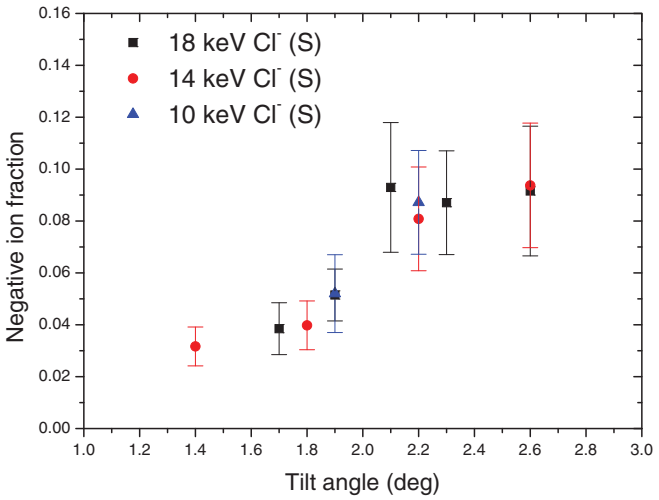

FIG. 4. (Color online) Negative ion fraction of scattered Cl^- from the *S* peak as a function of the tilt angle for different incident energies.

convolution of the beam divergence, capillary aspect angle, and capillary nonparallelism. The nonparallelism could lead to direct transmission even when the nanocapillaries are tilted to large angles, which was also found in the case of the HCI transmission [1,15].

Accompanying with the direct transmission, the scattering event associated with projectile neutralization indeed takes place in our case. The neutralization of multiply charged ions was recently reported by Stolterfoht *et al.* for Ar^{7+} ions in collisions with PET nanocapillaries [6] and is always accompanied with the guided HCIs. As an example, we plot our data for 18 keV Cu^- as shown in Fig. 5. The deflection angle θ, corresponding to the centroid of the peak position of scattered neutrals (see Fig. 1), increases linearly with the increase of the tilt angle ψ. Also drawn in Fig. 5 is a solid line where the deflection angle is equal to the tilt angle. The full circles almost fall on the solid line. As in the previous study of O^0, this behavior of the scattered neutrals (Cu^0 and Cl^0) from the *S*

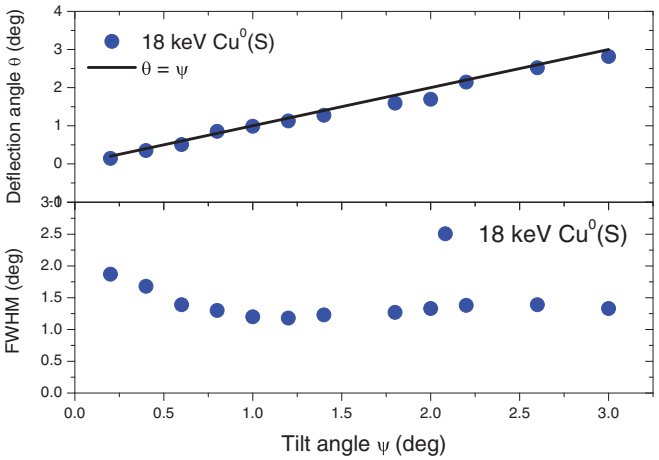

FIG. 5. (Color online) The centroid deflection angle (upper panel) and the FWHM (lower panel) vs. tilt angle for scattered Cu^0 ions when 18 keV Cu^- ions were transmitted through the nano-capillaries. The solid line shown in upper panel is drawn to show where the deflection and tilt angles are equal.

peak shows the so-called guiding phenomenon at equilibrium. The bottom panel in Fig. 5 presents the FWHM of the scattered Cu^0 as a function of the tilt angle. The FWHM goes down first ($\psi < 0.5°$), and then remains nearly constant (about 1.3°). The higher values of the FWHM at smaller angles result from the very small amount of scattered neutrals accumulated, which has a broad distribution structure leading to a poor statistic. The stabilization of the FWHM of neutrals suggests that neutrals are limited within a narrow grazing angular range.

The incoming negative ions suffer several small-angle collisions (deflection up, then down) with the inner surface atoms of the capillary at a grazing incidence and, at the same time, undergo the efficient neutralization at the scattering center along the zigzag trajectory. The charge transfer process (electron capture or loss) will continue until the neutrals exit the capillaries. This tentative scenario resulting from Fig. 5 reveals essential features: (i) the scattered neutrals are transported by the nanocapillaries through multiple grazing-angle scattering events [6,10,16] and (ii) the geometrical restrictions of the nanocapillaries determine the angular distribution of the scattered neutrals. This differs greatly from the *guiding effect* for transmitted HCIs [1–4] where HCIs are governed by the electrical field induced by *positive* charge patches on the capillary inner walls. With increasing the tilt angle, the scattering contribution to the transmitted particles becomes dominant and neutralization takes place efficiently. Moreover, we have not observed the scattered Cu^- ions (see Fig. 1). Even if the *negative* charge patch may be formed inside the capillaries, it is not able to repulse and guide negative ions efficiently. These provide us an obvious evidence of the absence of a guiding effect for negative-ion incidence.

To our knowledge, the charge-up phenomenon is a bad factor in the field of ion insulating-surface scattering. As a result, the experimental results cannot be reproduced well. Since no macroscopic charge-up occurs, in our case, the charge exchange process should be studied in detail. It can help us probe the inner surface electronic properties.

Now, let us first discuss the neutralization process. Destruction of negative ions in front of insulator surfaces has not been well understood so far. A number of different mechanisms of electron loss from the negative ion have been proposed to explain some of the experimental results, such as electron promotion [17], resonant ionization [18], resonant coherent ionization [19], and so on. Several studies [20,21] revealed to us the effect of projected band gap and surface image states on the neutralization of a negative ion approaching a noble-metal surface. As the ion approaches the surface, its affinity level is initially shifted downward due to the image potential effect and is then energetically repelled by the surface state and valence band states and, finally, arrives close to the image states near the bottom of the conduction band. In this way, the electron from the negative projectile is promoted and transferred to surface (image) states and the conduction band and thereby will progressively favor the decay through the bulk. In the case of an insulator surface with a wide band gap, it is expected that there will be less probable electron loss than metallic surfaces. However, Ustaze *et al.* [13] reported the observation of the existence of an efficient electron loss channel for atoms and anions under a grazing angle of incidence from an MgO (100) surface, where the memory of the initial charge state of

the projectile was lost completely at larger impact velocities (>1.5 keV) for fluorine projectiles with different charge states. Electron loss due to the nonadiabatic character of the electron transfer process was proposed. Compared to metallic surfaces, surface states inside the band gap of the insulator do not exist [22]. Thus, an electron decay to the surface state becomes impossible and hence the destruction may be ascribed to the up-shift of the Cu^- (Cl^-) level to the conduction band of Al_2O_3, which is assisted by a sufficiently close approach to the anion site with enough kinetic energy. As the tilt angle increases, more transmitted particles undergo scattering on the inner walls, resulting in increasing amounts of scattered neutrals.

The electron loss probability is expected to be higher for Cu^- ions, since these have the lower electron affinity. Of course, the final neutralization probability is related to the competition between electron loss and capture processes, which will be discussed below. The neutralization plays an important role here, at least, and is also an efficient intermediate for the production of negative and positive ions.

B. Negative-ion formation

For grazing atom-insulator surface scattering, charge transfer processes are very complicated because the relevant mechanism cannot be simply adopted from concepts derived for metals, since electron loss and capture are strongly suppressed by the wide band gap of the insulator. In addition, the parallel velocity effect, resulting from concepts of a modified Fermi sphere [10] in momentum space, may lead to the kinematically assisted negative-ion formation on metallic surfaces. However, this free electron picture of the shifted Fermi model is not appropriate in the case of insulating surfaces. Indeed, the negative ion formation on insulator surfaces is also favored by the parallel velocity effect via bridging the energy gap. The negative-ion formation is an inverse process of destruction of the negative ion mentioned above. For reference, a schematic energy-level diagram of the wide-band-gap insulator, target valence and conduction bands, and atomic levels of the investigated projectiles is shown in Fig. 6. The upper valence band is derived from O $2p$ states and the conduction band is derived from Al $3s$ and $3p$ states. The band gap of α-Al_2O_3 is about 8.7 eV and extends to vacuum energies [23]. In addition, the electron affinities of Cu^- (−1.23 eV), O^- (−1.46 eV), and Cl^- (−3.62 eV) and the first ionization energies of the corresponding particles (Cu, 7.73 eV; O, 13.62 eV; and Cl, 12.97 eV) studied are also shown in the figure [24].

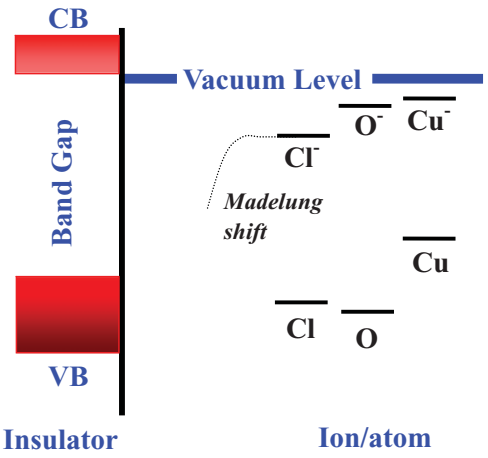

FIG. 6. (Color online) Schematic energy-level diagram of the Al_2O_3 target and affinity and the first ionization levels of O, Cu and Cl projectiles.

For negative-ion formation, we consider the projectile A^{q+} in front of the insulator surface located at a fixed distance of R. Interactions of incident particles with insulator surfaces have similarities to gas-phase collisions, which are obviously of a local character. The energy defect for electron capture in a binary type of collision from anion sites is given by Borisov and Sidis as [25],

$$\Delta E(\vec{R}) \approx \Delta E^{\text{binding}} + E_{\text{Mad}} + \frac{q-1}{R}, \quad R \gg a, \qquad (1)$$

where a is the crystal lattice constant, $\Delta E^{\text{binding}}$ the difference in binding energy of an electronic level in the valence band and the final atomic level, E_{Mad} the Madelung potential [12,25] created by the ionic lattice at active sites, and $\vec{R}$ the separation between the projectile A^{q+} and the anion site O^{2-}.

Let us first consider the case of negative-ion formation from the neutral projectile so $q = 0$ is the initial projectile charge. The increase of the tilt angle corresponds to the increase of the perpendicular velocity component with respect to the surface. As a result, the projectile approaches closer to the surface, and the attractive term $(-1/R)$ in Eq. (1) then initiates the confluence of energy levels of the negative projectile and the valence band states of the surface, resulting in the formation of negative ions. On the other hand, since the electron affinity of Cu^- is smaller than that of O^- and Cl^-, the initial energy gap $\Delta E(\vec{R})$ of Cl^- is the smallest, whereas that of Cu^- is the highest. Thus, it enhances the suppression of negative Cu^- ion formation. Furthermore, for a given incident energy, the Cu velocity is smaller than Cl, so the interaction time is long enough to complete the decay process. Based on the discussion above on the decay of negative ions in front of an insulator surface, the electron loss for Cu^- proceeds more efficiently than for O^- and Cl^- ions. Therefore, a higher fraction of Cl^- than Cu^- may be expected. Moreover, as the tilt angle increases, the number of collisions with the walls of the nanocapillaries increases, which enhances the probability of electron loss from negative ions formed in former collisions. Consequently, we could conclude that these factors support the absence of scattered Cu^- ions in the measurements.

It is also to be expected that, instead of producing negative ions from neutrals, the rise of negative ions from positive ions may be due to the opening of the double electron capture channel. The recent study of F^+ on a LiF(001) surface at grazing incidence revealed the evidence of F^- formation by simultaneous double electron capture from two adjacently active anion sites, which is not observed until the incident velocity is less than 0.1 a.u. [26]. In fact, double even *multielectron* capture processes are extensively studied for a single collision in multiply charged ion-atom collisions in the low-energy range [27–29], where the classical molecular over-the-barrier (CMOB) model provides us a distinct physical scenario [28,30]. In addition, for the interaction of multiply

charged ions with the metallic surface, the modified classical over-the-barrier (COB) model by Burgdörfer [31] is very suited to describe the stepwise neutralization of the projectile above the surface and agrees well with experiment.

The inelastic interaction involves the excitation of an electron from the valence band to higher-lying levels, resulting in the exciton formation. The production of surface excitons and the density of states may play some roles and finally affect the formation of negative ions. Such a surface exciton has been supported experimentally in collisions of hydrogen with a LiF surface [32]. The exciton binding energy can be on the order of 1000 meV and lies well below the affinity level of hydrogen relative to the vacuum level, so the electron excited from the valence band enables population of the surface exciton state prior to the affinity level and reduces the probability of negative-ion formation. However, to the best of our knowledge, only these core excitons observed experimentally are due to $2p^6 \rightarrow 2p^5 3s^1$ transitions in the cations [33] induced by swift electrons incident at Al_2O_3. For Al_2O_3, the core-exciton binding energy is normally less than 1000 meV [33] at room temperature and lies above the projectile's affinity level if the corresponding exciton could be formed in our case. Furthermore, it is less likely to recapture an electron from surface exciton states to projectile states, unless the exciton state is localized in the gap and is long lived.

C. Positive-ion production

Let us consider a singly charged ion approach to the surface, $q = 1$; the last term on the right-hand side of Eq. (1) disappears and the energy defect is replaced with $(\Delta E^{\text{binding}} + E_{\text{Mad}})$, which corresponds to the neutralization of singly charged ions. No confluence of energy levels between the negative ion and valence band states occurs [34]. In our case, the O and Cl ionization levels lie in close resonance with the valence band of the target, as shown in Fig. 6. Thus, the neutralization of singly charged ions is, as expected, more efficient for O^+ and Cl^+ than for Cu^+. In contrast, the ionization of Cu is easier than for Cl and O atoms because of its lower binding energy.

Next, we consider the ideal case of the direct transmission with a tilt angle of 0°, where transmitted positive ions can also be neutralized although these ions move in parallel with the capillary axis. According to the COB model mentioned above [31], the critical distance $d_c \approx \sqrt{2q}/W_\phi$ for charge transfer can be estimated, where q is the charge of the projectile ion and W_ϕ is the work function of a metal surface. In our case, the effective work function can be estimated approximately 4 eV [35]. With this estimation, we can calculate the radius for electron capture and resulting neutralization fraction from the ratio between the capture radius and the capillary radius [36], $2d_c/r \approx 4.1\%$. Of course, the work function of these capillaries is not known, since no well-defined stoichiometric composition of the material was used and the experiments were not carried out in ultra-high-vacuum conditions, where surface adsorbates could affect the work function.

We now return to the positive ion production from scattered neutrals, corresponding to the electron loss process. Distinct kinematic features are presented in Fig. 3. The positive ion could be produced through inelastic binary collisions with the surface atoms. For a projectile with incident energy E_p, a variation of the tilt angle ψ, corresponds to the change in a vertical energy $E_\perp = E_P \sin^2 \psi$. The probability of electron loss is enhanced when the projectile approaches the target atom much closer as both the incident energy E_p and tilt angle ψ increase. It should be noted that the ionization probability generally increases with increasing the kinetic energy and even the tilt angle with a small value shown in Fig. 3 can yield ionization of $Cu^0(Cl^0)$ with a large probability if the kinetic energy reaches larger than 10 keV.

V. CONCLUSION

In summary, we have performed a study of chlorine and copper transmitted through the Al_2O_3 nanocapillaries. It can be concluded that the guiding effect is not observed in our measurements, since electron capture and loss processes take place efficiently in the transmission; moreover, no Cu^- ion was formed. In particular, the scattered neutrals are transported along the capillary axis due to multiple grazing scattering [6,10,16], which differs from the guiding of HCIs. In fact, the formation of negative-charge patches on the capillary walls is affected strongly by material properties, such as surface conductivity, which, in turn, is influenced by surface adsorption properties and is difficult to control and quantify for nanocapillaries. Its importance has been reported very recently to explain the absence of ion blocking for PET [37]. Charge exchange, therefore, could be considered a useful tool to probe and characterize inner surface properties.

Due to the low ion beam dose and charge state of the projectile, the negative-charge deposition would have not yet been accomplished, just like in ion-insulating surface scattering one normally uses a low beam current to perform the measurement to avoid charging [38]. This allows us to study detailed characteristics of the charge-transfer processes for negative ions colliding with insulating nanocapillaries. A large yield of neutrals was observed, and the destruction of negative ions could be ascribed to the up-shift of Cu^- (Cl^-) level to the conduction band of Al_2O_3. The production of positive ions was also observed, which is attributed to inelastic binary collisions with the surface atoms. For negative ion formation, in contrast to chlorine, no Cu^- was observed, which is ascribed to its lower binding energy so efficient loss to the conduction band is possible.

We expect that, this work will stimulate theoretical analysis of the electron loss mechanism in the interaction of negative ions with insulator surfaces. One of the potential applications is to develop controlled neutral and negative beams without the deterioration of the ultra-high-vacuum (UHV) condition. On the other hand, the open question on the charge-up remains for future studies, the answer to which is still unclear. We suggest a possible way via enhancing beam currents and choosing other insulating materials by considering the properties of their surface conductivities.

ACKNOWLEDGMENTS

L. Chen gratefully acknowledges Professor Vladimir Esaulov for reading and comment on the manuscript. The

authors thank Zicun Chen and Lanting Li for preparing and tuning the ion source. This work was supported by the National Natural Science Foundation of China (Grant Nos. 10775063 and 11104124) and the Fundamental Research Funds for the Central Universities (Grant Nos. lzujbky-2010-27 and lzujbky-2010-29).

[1] N. Stolterfoht, J.-H. Bremer, V. Hoffmann, R. Hellhammer, D. Fink, A. Petrov, and B. Sulik, Phys. Rev. Lett. **88**, 133201 (2002).
[2] N. Stolterfoht, R. Hellhammer, J. Bundesmann, D. Fink, Y. Kanai, M. Hoshino, T. Kambara, T. Ikeda, and Y. Yamazaki, Phys. Rev. A **76**, 022712 (2007).
[3] N. Stolterfoht, R. Hellhammer, D. Fink, B. Sulik, Z. Juhász, E. Bodewits, H. M. Dang, and R. Hoekstra, Phys. Rev. A **79**, 022901 (2009).
[4] P. Skog, H. Q. Zhang, and R. Schuch, Phys. Rev. Lett. **101**, 223202 (2008); H. Q. Zhang, P. Skog, and R. Schuch, Phys. Rev. A **82**, 052901 (2010).
[5] A. Cassimi *et al.*, Nucl. Inst. Methods B **267**, 674 (2009).
[6] Z. Juhász, B. Sulik, R. Rácz, S. Biri, R. J. Bereczky, K. Tőkési, Á. Kövér, J. Pálinkás, and N. Stolterfoht, Phys. Rev. A **82**, 062903 (2010).
[7] Chen Yifeng *et al.*, Chinese Physics B **18**, 7 (2009).
[8] Xi Fayuan *et al.*, Chinese Physics B **18**, 5 (2009).
[9] Sun Guang zhi *et al.*, Phys. Rev. A **79**, 052902 (2009).
[10] H. Winter, Phys. Rep. **367**, 387 (2002).
[11] A. G. Borisov and V. A. Esaulov, J. Phys.: Condens. Matter **12**, R177 (2000).
[12] H. Winter, Prog. Surf. Sci. **63**, 177 (2000).
[13] S. Ustaze, R. Verucchi, S. Lacombe, L. Guillemot, and V. A. Esaulov, Phys. Rev. Lett. **79**, 3526 (1997).
[14] Stefan A. Deutscher, Andrei G. Borisov, and Victor Sidis, Phys. Rev. A **59**, 4446 (1999).
[15] N. Stolterfoht, R. Hellhammer, P. Sobocinski, Z. D. Pešic, J. Bundesmann, B. Sulik, M. B. Shah, K. Dunn, J. Pedregosa, and R. W. McCullough, Nucl. Inst. Methods Phys. Res. B **235**, 460 (2005).
[16] H. F. Krause, C. R. Vane, and F. W. Meyer, Phys. Rev. A **75**, 042901 (2007).
[17] P. A. Zeijlmans van Emmichoven, A. Niehaus, P. Stracke, F. Wiegershaus, S. Krischok, V. Kempter, A. Arnau, F. J. García de Abajo, and M. Peñalba, Phys. Rev. B **59**, 10950 (1999).
[18] H. Winter, C. Auth, and A. G. Borisov, Nucl. Inst. Methods Phys. Res. B **115**, 133 (1996).
[19] H. Winter, A. Mertens, and C. Auth, Phys. Rev. A **54**, 2486 (1996).
[20] T. Hecht, H. Winter, A. G. Borisov, J. P. Gauyacq, and A. K. Kazansky, Phys. Rev. Lett. **84**, 2517 (2000); A. G. Borisov, A. Mertens, S. Wethekam, and H. Winter, Phys. Rev. A **68**, 012901 (2003).
[21] Himadri Chakraborty, Thomas Niederhausen, and Uwe Thumm, Phys. Rev. A **70**, 052903 (2004); Andrew Schmiz, John Shaw, Himadri Chakraborty, and Uwe Thumm, *ibid.* **81**, 042901 (2010).
[22] A. Mertens, C. Auth, H. Winter, and A. G. Borisov, Phys. Rev. A **55**, R846 (1997).
[23] Shang-Di Mo and W. Y. Ching, Phys. Rev. B **57**, 15219 (1998).
[24] V. Esaulov, Ann. Phys. Fr **11**, 493 (1986).
[25] C. Auth, A. Mertens, H. Winter, A. G. Borisov, and V. Sidis, Phys. Rev. A **57**, 351 (1998).
[26] P. Roncin, A. G. Borisov, H. Khemliche, A. Momeni, A. Mertens, and H. Winter, Phys. Rev. Lett. **89**, 043201 (2002).
[27] C. Harel, H. Jouin, and B. Pons, J. Phys. B: At. Mol. Opt. Phys. **24**, L425 (1991).
[28] M. Barat and P. Roncin, J. Phys. B: At. Mol. Opt. Phys. **25**, 2205 (1992).
[29] Wolfgang Fritsch and C. D. Lin, Phys. Rev. A **45**, 6411 (1992).
[30] A. Niehaus, J. Phys. B: At. Mol. Opt. Phys. **19**, 2925 (1986).
[31] Joachim Burgdörfer, Peter Lerner, and Fred W. Meyer, Phys. Rev. A **44**, 5674 (1991).
[32] P. Roncin, J. Villette, J. P. Atanas, and H. Khemliche, Phys. Rev. Lett. **83**, 864 (1999).
[33] W. L. O'Brien, J. Jia, Q.-Y. Dong, T. A. Callcott, D. L. Mueller, D. L. Ederer, N. D. Shinn, and S. C. Woronick, Phys. Rev. B **44**, 13277 (1991); W. L. O'Brien, J. Jia, Q.-Y. Dong, T. A. Callcott, D. R. Mueller, and D. L. Ederer, *ibid.* **45**, 3882 (1992).
[34] A. G. Borisov and V. Sidis, Phys. Rev. B **56**, 10628 (1997).
[35] Weijie Song and Michiko Yoshitake, Appl. Surf. Sci. **251**, 14 (2005).
[36] S. Ninomiya, Y. Yamazaki, F. Koike, H. Masuda, T. Azuma, K. Komaki, K. Kuroki, and M. Sekiguchi, Phys. Rev. Lett. **78**, 4557 (1997).
[37] N. Stolterfoht, R. Hellhammer, B. Sulik, Z. Juhász, V. Bayer, C. Trautmann, E. Bodewits, and R. Hockstra, Phys. Rev. A **83**, 062901 (2011).
[38] S. Ustaze, R. Verucchi, S. Lacombe, L. Guillemot, and V. A. Esaulov, Phys. Rev. Lett. **79**, 3526 (1997).